CrystEngComm

Cite this: *CrystEngComm*, 2011, **13**, 3967

www.rsc.org/crystengcomm

COMMUNICATION

Controlled growth of the silicide nanostructures on Si bicrystal nanotemplate at a precision of a few nanometres

Cheng-Lun Hsin,[ab] Wen-Wei Wu,*[b] Li-Wei Chu,[a] Hung-Chang Hsu[a] and Lih-Juann Chen*[a]

Received 17th March 2011, Accepted 15th April 2011
DOI: 10.1039/c1ce05329a

A nanotemplate of Si bicrystal was fabricated by wafer bonding. The surface electronic energy arrangement on the surface of the Si bicrystal has been measured by scanning tunneling microscopy. The stress effect on the stepped growth of titanium silicide nanorods on Si bicrystal was observed in an ultrahigh vacuum transmission electron microscope in real time. The growth behavior of the nanorods was found to be affected by the underlying dislocation arrays significantly. For a dislocation interspacing of 3.1 nm, the dislocation arrays confined the shape of the nanoclusters and nanorods. Compared to the time of the nanorod remaining at the same length, the elongating time is more than two orders of magnitude shorter. The stepped growth behavior is attributed to the stress contour of the surface strain induced by the underlying dislocation network. This study is constructive to the basic understanding of the stress effect on the initial stage of the reaction of metals on Si and the observation may be applied to nanostructure growth for future applications and design.

Introduction

Nano-scaled growth has been the subject of intensive research for many years. Recent studies have been focused on the investigation of the nucleation and growth mechanisms since the control of the nanostructure is an important issue for future applications of the unique properties of the nanomaterials.[1–4] With high regularity and controllable dislocation interspacing (DI) of several tens of nanometres below the surface, silicon bicrystal has been a model template for surface control and dynamic reaction study. There have been a few works on the fabrication of silicon bicrystals and the fundamental nature of the induced strain by theoretical basis.[5–11] The characteristics of dislocation networks and the surface strain have been investigated. The underlying dislocation network plays a critical role on the surface energy and the induced stress leads to the variation in surface strain field. Therefore, the dislocation networks would have significant influences on the top nanostructures.[12–15] Although the stress effect has been studied through the formation of nanostructures on the surface of the bicrystal, the growth behavior of the nanomaterial on the bicrystal is still unclear. Here, the real time observation of the nanostructures under the effect of strain provides fundamental understanding of growth dynamics, which is the key factor in controlling the nanostructures for their future applications.

Metal silicides have been widely used in the microelectronic industry as contacts and gate electrodes. The reactions between metal and silicon have been of much interest in the past three decades.[16–18] Among them, titanium silicides have been extensively investigated in recent years and the study of the nucleation and growth behaviors of titanium silicides has been conducted.[19] Thus, the clarification of the growth of silicide nanowires on Si bicrystal would be a significant advance to understand the reaction with the effect of surface stress. With the powerful applications of the scanning tunneling microscope (STM) and *in situ* ultra-high-vacuum transmission electron microscope (UHV-TEM),[20] the surface strain effect on the surface energy arrangement and the growth of silicide nanostuctures can be investigated. In this work, we report the results of investigations on the surface energy and the dynamic growth of Ti silicide nanorods on the silicon bicrystal. The dislocation network confined the nanorod to match the dislocation grids during the growth process and the stepwise growth of the nanorod by one grid spacing was observed. The crucial observation would elucidate stress effect on nanostructure growth and be applied to grow nanowires with desired length.

Experimental methods

The silicon bicrystal was fabricated *via* silicon wafer bonding of a (001) silicon wafer and a (001) silicon on insulator (SOI) wafer with a 30 nm-thick top silicon layer. The procedures for the fabrication and the formation mechanism of the dislocation array were illustrated in Fig. 1. The silicon and SOI substrates were chemically cleaned using a standard RCA process followed by dilute HF dipping to produce clean and hydrophobic silicon surfaces. The wafers were bonded at room temperature at a controlled twist angle and annealed at 1100 °C subsequently for 1 h to form the dislocation array at the bonding interface. A mechanical grinding and chemical etching technique was used to remove the backside silicon substrate of the SOI wafer. The silicon oxide was then removed with a dilute HF etching. Si bicrystal with DI of 3.1 nm was prepared. The surface topography was examined in the STM. The samples were annealed at

[a]*Department of Materials Science and Engineering, National Tsing Hua University, No. 101, Section 2, Kuang-Fu Road, Hsinchu, Taiwan, 30013, R.O.C. E-mail: wwwu@mail.nctu.edu.tw; ljchen@mx.nthu.edu.tw; Fax: +886-3-5724727; Tel: +886-3-5712121-55395*
[b]*Department of Materials Science and Engineering, National Chiao Tung University, No.1001, University Rd., East Dist., Hsinchu, Taiwan, 30013, R.O.C.*

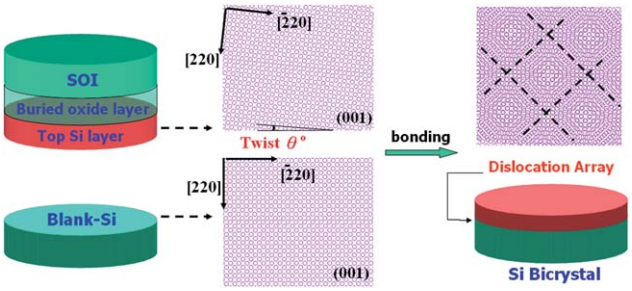

Fig. 1 Schematic illustration of the fabrication process for the Si bicrystal and the formation mechanism of the dislocation array.

600 °C for several hours and flashed several times at 1200 °C for a total of 1 min at 2×10^{-9} Torr. *In situ* transmission electron microscope (TEM) examinations were conducted in an UHV-TEM with a base pressure of 3×10^{-10} Torr. Prior to the *in situ* TEM observation, the sample was placed into a heating holder for degassing and flashing in the pretreatment chamber. During the observation, Ti was deposited on the samples at a rate of 0.07 nm min^{-1} by electron beam evaporation in the UHV-TEM. The real time observations were carried out at 700 °C and the video recorder has a time resolution of 1/30 s.

Results and discussion

Fig. 2(a) shows a TEM image of Si bicrystal with DI of 3.1 nm corresponding to a twist angle of 6.5 deg. With no interference of the miscut dislocation, the dislocation array is well arranged. Both the primary and secondary diffraction spots were depicted in the diffraction pattern, as shown in Fig. 2(b). The DI can also be inferred from the spacing between primary and secondary spots of the diffraction spots. The Si bicrystal in Fig. 2(a) was the standard template to study the stress effect on the growth of the silicide nanorods in real time. The STM image of the Si bicrystal was revealed in Fig. 2(c). Remarkably, a regularly distributed surface roughness (highlighted by the green-dashed lines) was observed, indicating that the stress of the underlying screw dislocation array has influence on the surface electronic distribution. The STM tip position on the top region of the dislocation array was 0.01 nm higher, proving that the surface energy distribution induced by the dislocation array was detected and the accumulated surface electron density could be found on the top of the dislocation array.

In the *in situ* TEM experiments on the bicrystal substrate, silicide nanorods were formed. Significantly, the morphology of the titanium silicide nanostructures was found to be affected by the induced stress of the dislocation array, as shown in Fig. 3(a). The shape was not only confined into orthogonal rectangle, but the edges were also located on the dislocation lines. The inset in Fig. 3(a) is the corresponding electron diffraction pattern of the nanorod. Due to the shorter height and smaller dimension of the nanorods grown on the substrate, diffraction spots were weaker and only few spots with stronger signals rather than multiple sets of clear diffraction spots were seen from the screen. However, based on computational modeling and analysis for the Ti–Si system, only the $(3\bar{1}\bar{2})$ and (204) plane of the tetragonal Ti_5Si_4 phase would match the simulated pattern. For comparison, on blank Si under the same growth condition, only nanoclusters with random shapes were formed. An example is shown in Fig. 3(b).

The micrographs presented in Fig. 4 were reproduced from video images of the silicide grown from 11 grids to 14 grids (see case 1 in Fig. 5). The DI of the images is 3.1 nm. At the beginning of the recording, the nanorod was of three grids in width and 11 grids in length, as shown in Fig. 4(a). After 45 seconds (Fig. 4(b)), the nanorod extended to 12 grids in length within 1 s (Fig. 4(c)). Then, the nanorod maintained the same length up to 292 s until the image of the nanorod became more prominent. Subsequently, the nanorod elongated again from 12 to 13 grids within a second, as shown in Fig. 4(d) and (e). Similarly, the nanorod grew from 13 grids to 14 grids within a second at 455 s, as depicted in Fig. 4(f) and (g). These repeating events show the step-wise growth of the nanorod. From 456 s to 969 s, the nanorod kept the same shape and the contrast of the image improved (Fig. 4(h)). It is believed that the nanorod had increased the thickness to lower the total free energy during the growth time. This observation demonstrated that the length of the silicide nanorod can be intentionally controlled by the unit of the DI. Furthermore, because the video recorder has a time resolution of 1/30 s, we can obtain 30 images to investigate the growth dynamics of the nanorod within 1 s. For these 30 images from the 455 s to 456 s, which the nanorod kept 3 grids in width but elongated to 14 grids in length, the analysis of these images shows that the growth front was covered step by step from the first grid to the third grid at the end.

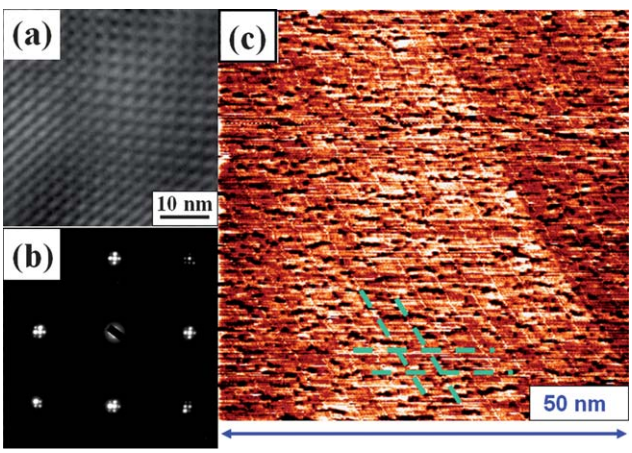

Fig. 2 (a) TEM images of the as-prepared Si bicrystal nanotemplate, (b) corresponding electron diffraction patterns, and (c) STM image of the Si bicrystal. Inset shows the high magnification STM image of Si(001)-2 × 1 reconstructed surface and the green-dashed lines highlighted the surface topography.

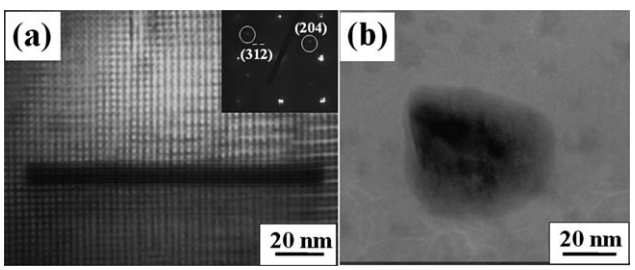

Fig. 3 TEM images of the Ti silicide grown on (a) Si bicrystal and (b) blank Si, respectively. Inset in (a) shows the corresponding selective area electron diffraction pattern of the nanorod.

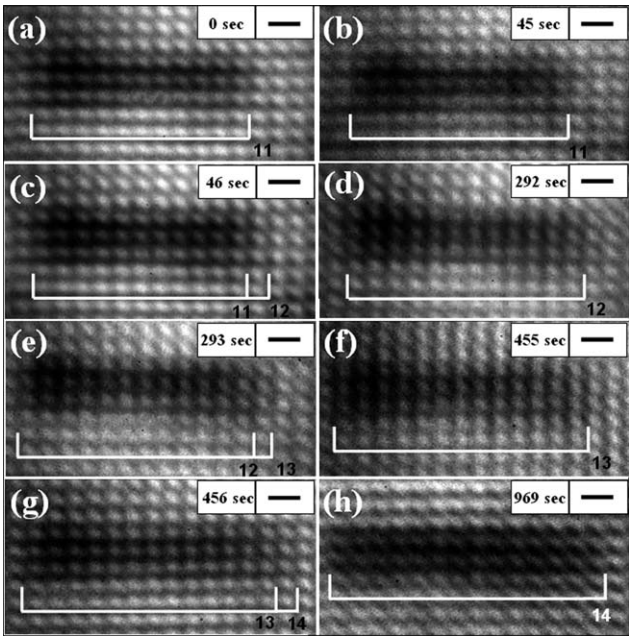

Fig. 4 A series of images showing the stepwise growth of the Ti silicide nanorod on Si bicrystal at 700 °C. The images were obtained at elapsed times of (a) the initial of the recording, (b) 45 s, (c) 46 s, (d) 292 s, (e) 293 s, (f) 455 s, (g) 456 s, and (h) 969 s. Scale bar in the inset represents 5 nm. The white lines and the numbers at the bottoms highlighted the length of the nanorod in number of dislocation spacing.

These images illustrated that the growth at the elongated front still affected by the surface stress and confined by the dislocation grids.

The plot of the stepwise growth of the nanorods by number of grids in length as a function of time is shown in Fig. 5. Another example (case 2) of the growth of the nanorod from 21 grids to 25 grids is also exhibited. Based on the result in Fig. 5, the average time periods of the two cases maintaining at the same length are 205 s and 215 s, respectively. This indicates that the elongating time of the nanorods is commensurate and is over two orders of magnitude shorter than the time maintaining the same length. These phenomena distinctly correlate to the effect of the confinement of the surface stress.

For the sample with blank Si, the stepwise growth of the silicides was not observed. In addition, the morphology was random in shape and only nanoclusters were formed. With continuous Ti deposition, the size of the nanocluster grew gradually. However, there was no regularity observed during the process. It demonstrates that the confinement effect is originated from the surface stress to modulate the as-grown silicide to match the dislocation lines. These experimental results also suggest more appropriate and precise control of the length of the nanostructures by the Si bicrystals.

Fig. 6(a) is the TEM image showing that Ti was deposited on the sample at room temperature and then the sample was annealed at 700 °C for 1 h. Fig. 6(b) depicted the high-magnification TEM image of the nanocluster. There were only square silicide nanoclusters and no silicide nanorod formed on the bicrystal. Besides, the nanoclusters were confined by the dislocation array and the size of the nanoclusters was similar. This observation also indicates that the high surface stress region is the preferential site for nucleation. No stepwise-growth behavior was found during the subsequent observation due to the deficiency of the Ti atoms.

In our results, the induced stress restrains the nanocluster to be confined at the dislocation lines. Meanwhile, from the theoretical predictions,[21] the surface strain energy and the stress arrangement would affect the growth of the as-grown silicides at the surface. During the initial growth stage, Ti deposited on the surface would react with Si while the region with high surface stress would be more suitable for the nucleation of the as-grown silicide nanoclusters. The STM results in our study in Fig. 2(c) also show that the edge lines are the energetic minimum sites for nucleation. Thus, the nucleation time would be much shorter than the growth time, resulting in the stepwise growth. This growth behavior is similar with our previous report.[1] In addition, with the increase of the growth time, the nanocluster shall become larger and increase in volume. However, the dislocation confined the as-formed silicide at the edge line, *i.e.*, silicide tended to locate at the edge lines. As the up-coming Ti atoms react with the underlying Si to form silicide, the contrast of the silicide image will improve and the nanorod would grow. In our previous study of the growth of titanium silicide nanowires,[19] the increased length of the nanowire can be visualized by the moiré fringe (~1.38 nm), which is compatible with the DI of the bicrystal. With a short distance of the dislocation spacing, the progression of the silicide would reach the edge because of the favorable minimum energy. With these conditions, the growth period of the nanorod was relatively short

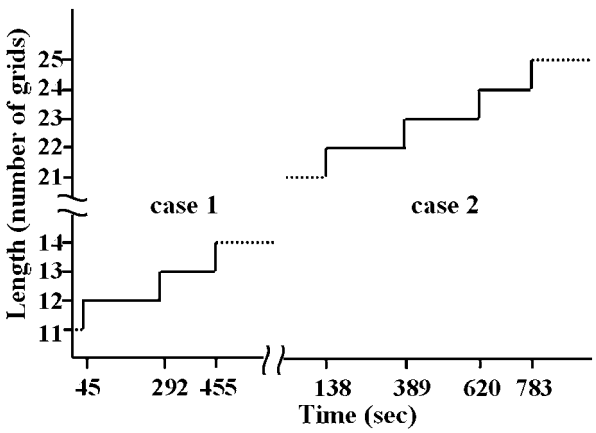

Fig. 5 Plot of the stepwise growth of the nanorods by number of grids in length as a function of time.

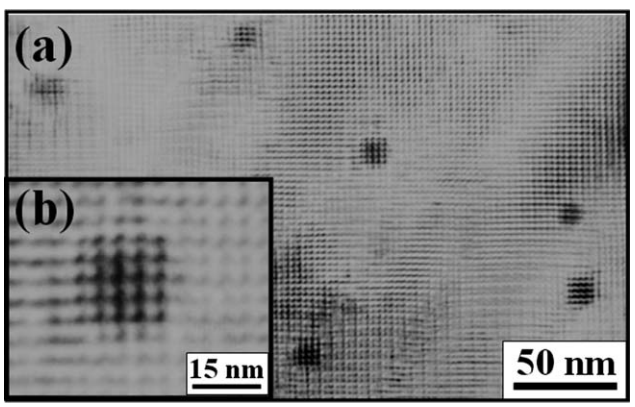

Fig. 6 (a) TEM images of the Ti silicide on Si bicrystal. Ti was deposited at room temperature and then the sample was annealed. (b) High-magnification TEM image of the nanocluster.

compared to the time that the nanorod maintained the same length. As a result, the nanorod grew in steps.

The average growth rate of the nanorods was observed to be about 13 times higher than the deposition rate. Thus, surface diffusion is also a crucial part for the growth of the nanorods. Ti deposited around the growing nanorods would diffuse to the nanorods to react with Si at high temperatures to increase the volume of the silicide. Thereby, the formation of the silicide nanorods is originated from the deposited and diffusing Ti atoms. On the other hand, orthorhombic and tetragonal Ti_5Si_4 may coexist at 700 °C if the amount of deposited Ti is low.[22] It was previously found that the decrease in film thickness would result in the increase of the formation temperature of C49–$TiSi_2$.[23]

Conclusions

In summary, we have fabricated the Si bicrystals nanotemplate with controlled DI and investigated the surface effect on the surface electronic energy arrangement by STM and the growth kinetics of the silicide nanorods by *in situ* UHV-TEM. The morphology of the nanorods was confined by the induced surface strain of the dislocation array. Therefore, nanorods with a desired width and length could be obtained. Step by step growth of the nanorod was observed and the silicide nanorod grew by one DI within a second at a substrate temperature of 700 °C. The stepwise growth mechanism is attributed to the surface strain energy and surface diffusion is also an essential part for the nanosilicide formation. The observation of the stress confinement of the growth of the nanostructure is potentially significant for applications in nanoscience and nanotechnology.

Acknowledgements

The authors W.W.W. and L.J.C. acknowledge the support from NSC Grants 97-2218-E-009-027-MY3, 99-2120-M-007-011 and 98-2221-E-007-104-MY3.

Notes and references

1 Y. C. Chou, W. W. Wu, S. L. Cheng, B. Y. Yoo, N. Myung, L. J. Chen and K. N. Tu, *Nano Lett.*, 2008, **8**, 2194.
2 K. C. Lu, W. W. Wu, H. W. Wu, C. M. Tanner, J. P. Chang, L. J. Chen and K. N. Tu, *Nano Lett.*, 2007, **7**, 2389.
3 K. Pohl, M. C. Bartelt, J. de la Figuera, N. C. Bartelt, J. Hrbek and R. Q. Hwang, *Nature*, 1999, **397**, 238.
4 C. Y. Wen, M. C. Reuter, J. Bruley, J. Tersoff, S. Kodambaka, E. A. Stach and F. M. Ross, *Science*, 2009, **326**, 1247.
5 W. Cai, V. V. Bulatov, J. P. Chang, J. Li and S. Yip, *Phys. Rev. Lett.*, 2001, **86**, 5727.
6 F. Fournel, H. Moriceau, B. Aspar, K. Rousseau, J. Eymery, J. L. Rouviere and N. Magnea, *Appl. Phys. Lett.*, 2002, **80**, 793.
7 L. B. Hansen, K. Stokbro, B. I. Lundqvist, K. W. Jacobsen and D. M. Deaven, *Phys. Rev. Lett.*, 1995, **75**, 4444.
8 R. A. Marks, S. T. Taylor, E. Mammana, R. Gronsky and A. M. Glaeser, *Nat. Mater.*, 2004, **3**, 682.
9 K. Rousseau, J. L. Rouviere, F. Fournel and H. Moriceau, *Appl. Phys. Lett.*, 2002, **80**, 4121.
10 G. Springholz and K. Wiesauer, *Phys. Rev. Lett.*, 2002, **88**, 015507.
11 R. A. Wind, M. J. Murtagh, F. Mei, Y. Wang, M. A. Hines and S. L. Sass, *Appl. Phys. Lett.*, 2001, **78**, 2205.
12 F. Leroy, J. Eymery, P. Gentile and F. Fournel, *Appl. Phys. Lett.*, 2002, **80**, 3078.
13 F. Leroy, G. Renaud, A. Letoublon, R. Lazzari, C. Mottet and J. Goniakowski, *Phys. Rev. Lett.*, 2005, **95**, 185501.
14 C. H. Liu, W. W. Wu and L. J. Chen, *Appl. Phys. Lett.*, 2006, **88**, 023117.
15 C. H. Liu, W. W. Wu and L. J. Chen, *Appl. Phys. Lett.*, 2006, **88**, 133112.
16 Y. C. Lin, K. C. Lu, W. W. Wu, J. W. Bai, L. J. Chen, K. N. Tu and Y. Huang, *Nano Lett.*, 2008, **8**, 913.
17 Y. P. Song, A. L. Schmitt and S. Jin, *Nano Lett.*, 2007, **7**, 965.
18 Y. Wu, J. Xiang, C. Yang, W. Lu and C. M. Lieber, *Nature*, 2004, **430**, 61.
19 H. C. Hsu, W. W. Wu, H. F. Hsu and L. J. Chen, *Nano Lett.*, 2007, **7**, 885.
20 K. C. Chen, W. W. Wu, C. N. Liao, L. J. Chen and K. N. Tu, *Science*, 2008, **321**, 1066.
21 A. Bourret, *Surf. Sci.*, 1999, **432**, 37.
22 H. F. Hsu, T. F. Chiang, H. C. Hsu and L. J. Chen, *Jpn. J. Appl. Phys.*, 2004, **43**, 4541.
23 H. Jeon, C. A. Sukow, J. W. Honeycutt, G. A. Rozgonyi and R. J. Nemanich, *J. Appl. Phys.*, 1992, **71**, 4269.

